SHARP: The SHARC-II Polarimeter for CSO

H. Li[a], M. Attard[b], C. D. Dowell[c], R. H. Hildebrand[d, e], M. Houde[b], L. Kirby[d], G. Novak[a],
and
J. E. Vaillancourt[d]

[a]Northwestern University, Dept. of Physics and Astronomy, Evanston, IL, 60208, USA
[b]University of Western Ontario, Dept. of Physics and Astronomy, London, ON, N6A 3K7, Canada
[c]Caltech/JPL, Pasadena, CA, 91109, USA
[d]University of Chicago, Enrico Fermi Institute and Department of Astronomy and Astrophysics, Chicago, IL, 60637, USA
[e]University of Chicago, Department of Physics, Chicago, IL, 60637, USA

ABSTRACT

SHARC-II is a 32 x 12 pixel submillimeter camera that is used with the ten-meter diameter Caltech Submillimeter Observatory (CSO) on Mauna Kea. This camera can be operated at either 350 or 450 microns. We developed a module that is installed at the CSO Nasmyth focus in order to convert SHARC-II into a sensitive imaging polarimeter, which we refer to as "SHARP". SHARP splits the incident beam into two orthogonally polarized beams that are then re-imaged onto different halves of the SHARC-II bolometer array. When this removable polarimetry module is in use, SHARC-II becomes a dual-beam 12 x 12 pixel polarimeter. Sky noise is a significant source of error for submillimeter continuum observations. Because SHARP simultaneously observes two orthogonal polarization components, we are able to eliminate or greatly reduce this source of error. Here we describe the design of SHARP and report preliminary results of tests and observations carried out during our first two runs at CSO in August 2005 and January 2006.

Keywords: Submillimeter, Polarimeter.

1. INTRODUCTION

The earliest detections of far-infrared/submillimeter polarization in astronomical objects were obtained using single-pixel polarimeters operated in the stratosphere, from balloons[1] and aircraft[2]. This work established a new technique for tracing the orientations of interstellar magnetic fields. During the 1990's, astronomers developed more powerful polarimeters with many tens of pixels. Two examples that were built at U. Chicago are Stokes[3] for the Kuiper Airborne Observatory (KAO), and Hertz[4, 5] for the Caltech Submillimeter Observatory (CSO) on Mauna Kea. These instruments gathered polarization data for more than a dozen star forming clouds, at up to several hundred sky positions per cloud, and discovered that dust emission is measurably polarized at almost every point[5, 6, 7, 8].

Another multi-pixel polarimeter that was developed during the 1990's is SCU-POL[9], the polarimeter for the Submillimeter Common-User Bolometer Array (SCUBA)[10], used with the James Clerk Maxwell telescope (JCMT) on Mauna Kea. SCU-POL has been used to map magnetic fields in many high and low mass star-forming regions as well as in the Galactic center. SCU-POL has also obtained the first detection of submillimeter polarization in circumstellar disks around T Tauri stars[11].

In the early 2000's, submillimeter polarimetry was extended to both larger and smaller angular scales. For example, the Submillimeter Array (SMA)[12] on Mauna Kea studied Sgr A* with sub-arcsec resolution[13], while Submillimeter Polarimeter for Antarctic Remote Observations (SPARO)[14] mapped the degree scale magnetic fields in the Galactic center[15] and giant molecular clouds located in the Galactic disk[16]. Cosmologists are interested in millimeter-wave polarimetry[17] as a probe of the early universe, and as a byproduct, they have already produced high quality maps of the global magnetic field of the Galaxy[18, 19].

Instead of building new polarimeters, it will be very efficient both in time and money if we can convert existing cameras into polarimeters. SHARP provides polarimetric capability for the SHARC-II[20] (Submillimeter High Angular Resolution Camera generation II) of the CSO by inserting a module into the optical train ahead of the cryostat (Fig. 1). The incoming beam is split into orthogonal components of polarization that are directed to opposite ends of the 32 x 12 pixel bolometer array (Fig. 2). The signals from the two components are recorded simultaneously. Let the two components be h and v. Then the polarization level can be measured by taking the ratio of their difference and sum

$$P = (h - v) / (h + v)$$

From this equation one can see that P is unaffected by changes in atmospheric transmission, and that fluctuations in emission are removed from the numerator. Although variations in emission are still included in the denominator, they are often small compared to the total signal intensity ($h + v$). (When they are not, the effects of such “sky noise” can cause large errors in P, but these can be avoided by using special techniques[21, 22].) In comparison with polarimeters like SCU-POL at the JCMT (now decommissioned awaiting SCUBA-2) that sample a single component at a time, dual-beam polarimeters gain a much higher signal to noise ratio because atmospheric fluctuations affect the two components equally and are thus largely cancelled during the analysis[5, 7, 21] (Fig. 3). Without simultaneous detection, the effects of sky noise are much worse at 350 and 450 µm than at 850 µm. For SHARP observations, we use standard infrared techniques[7] of spatially chopping the secondary mirror to remove the large atmospheric background and position switching the telescope to remove synchronous offsets.

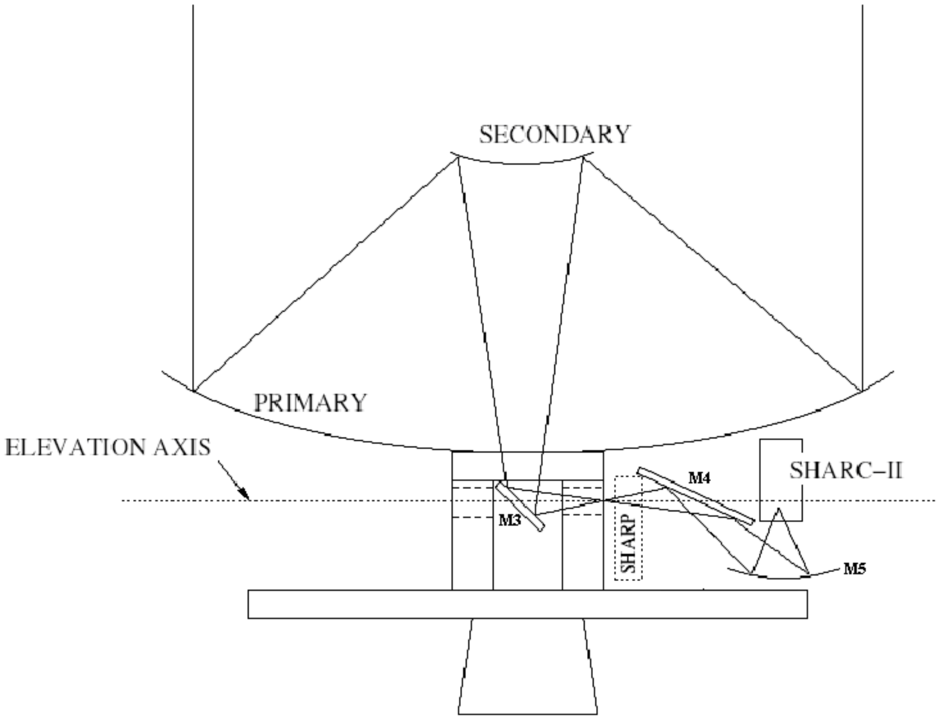

Fig. 1 Schematic drawing of SHARC-II on the Nasmyth platform (not to scale). A flat mirror (M3) below the secondary deflects the beam into the hollow elevation bearing, producing an image of the sky within the bearing. The location of the removable polarimetry module SHARP is shown.

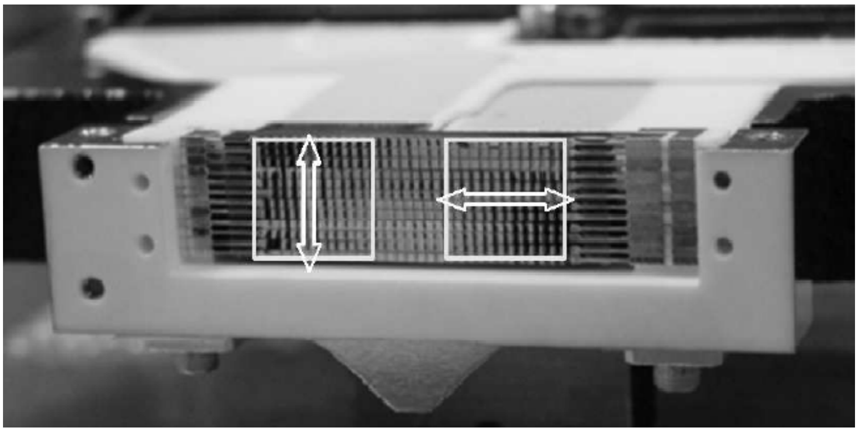

Fig. 2 Photograph of the SHARC-II detector array, with markings that illustrate the effect of the SHARP polarization-splitting optics. When SHARP is installed the detector array will effectively be converted into two 12×12 sub-arrays that view the same ~ 1’ × 1’ sky field in orthogonal polarizations.

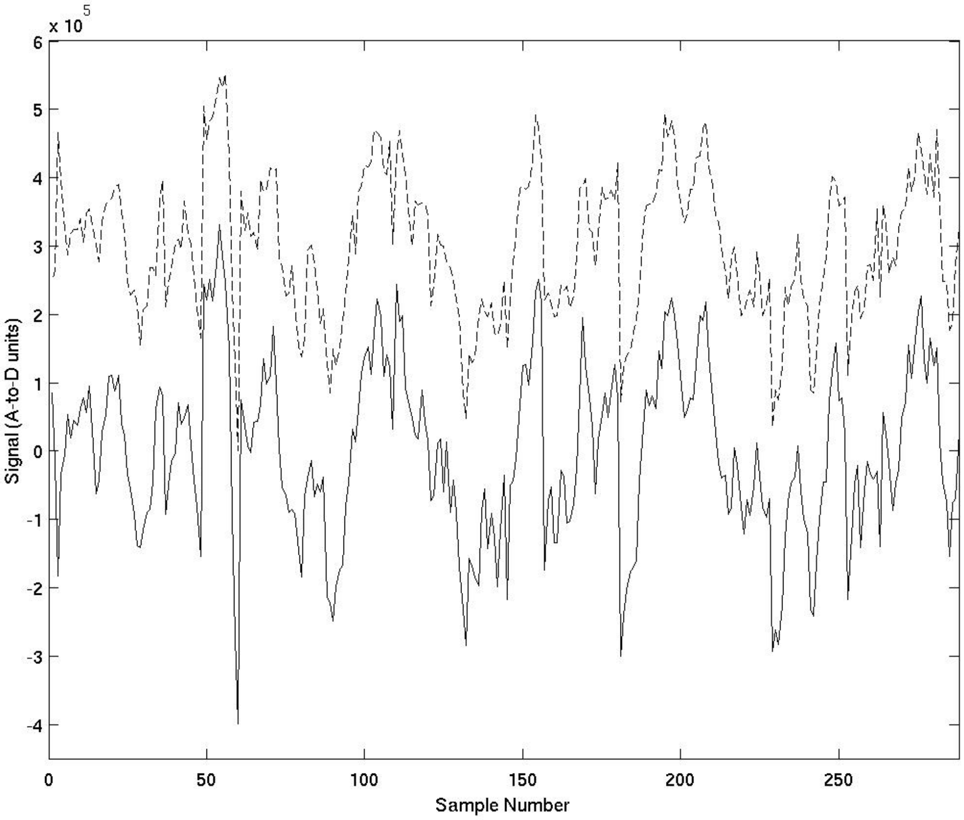

Fig. 3 Correlated sky noise at South Pole. This figure shows the result of an eight-minute integration obtained during Austral Winter 2003 with the SPARO experiment at South Pole[14, 15, 16]. The solid and dashed curves show the demodulated signals measured with two bolometers observing the same part of the sky in orthogonal linear polarizations. The dashed curve has been shifted upward for clarity. The signal from the astrophysical source, G333.6–0.2, was removed to better show the sky noise.

2. OPTICAL DESIGN

2.1 The CSO/SHARC-II optics

Before describing our polarimetry module, we review the optical interface between the CSO telescope and the SHARC-II camera. SHARC-II uses the Nasmyth focus of the CSO, as shown schematically in Figure. 1. It does not sit directly at the Nasmyth focus (~ f/12). Instead, this focus is re-imaged along a folded optical path ~2.5 m in length that includes a flat mirror (M4, Fig. 1) and an ellipsoidal mirror (M5, Fig. 1). The SHARC-II bolometer array is located at the re-imaged focal plane, which is faster (~f/4). An image of the primary (a “pupil”) is located several inches in front of this focus, and SHARC-II has a cold stop at this pupil.

2.2 Focal plane re-imaging

How can we introduce a series of optical components into an already optimized system without modifying the components of the original system and without degrading the performance? We have to increase the optical path of the original system for the new optical components, and at the same time, not move the original focal plane used by the detector array. We achieved this by introducing a pair of identical paraboloidal mirrors right after the Nasmyth focus (Fig. 4). The dual paraboloids[24] re-image the Nasmyth focus so that the new optical path between the original (f) and the re-imaged Nasmyth focus (f’) can be used for the polarimeter module. The new optical components are arranged so that the re-imaged Nasmyth focus will be relayed to a position that has exactly the same optical distance to the SHARC II detectors as the original Nasmyth focus had.

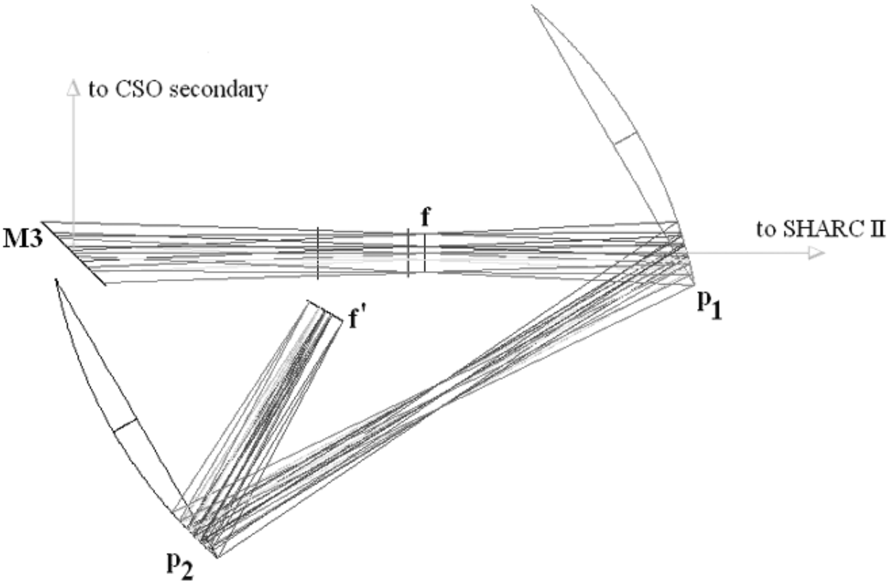

Fig. 4 Diagram showing the “unfolded” optical design, in order to illustrate our use of dual paraboloidal mirrors (P1and P2) to re-image the Nasmyth focus (f). The focus of the first mirror is placed on f, and f is re-imaged at f ’, the focus of the

second paraboloid, with minimal aberration[24]. Two important criteria used in the design are ∠fP1P2= ∠f'P2P1and having the pupil half-way between P1 and P2. All the polarimeter components are installed after P1, and besides separating the incident light into orthogonal components, they relay f ' to a position having the same optical distance to SHARC II as f had in the original SHARC-II optical path.

2.3 The polarimetry optics

The arrangements of polarimeter components are illustrated in Fig. 5. After P1, the first paraboloidal mirror, and the flat mirror (F1) is the half-wave plate module (HWP), which contains two rotatable and interchangeable crystal half-wave plates (for 350 and 450 μm, respectively) that are controlled by a stepping motor and monitored by an absolute encoder. HWP is installed near the pupil (Fig. 4, half-way between P1 and P2) to minimize the size of the plate (diameter ~ 10 cm) and to keep different portions in the field of view using the same part of the plate. Also near the pupil, for the same reasons, is the "crossed grid", XG (Fig. 7, commercially available from QMCI, Cardiff, Wales). The wire directions of the two wire grids in XG are perpendicular to each other and the two grids intersect at a right angle, so that XG divides the beam into two orthogonal linearly polarized components, which proceed in opposite directions (both perpendicular to the incident beam) toward the next two flat relay mirrors, F2h-F3h and F2v-F3v. (Here h (v) stands for the component which is horizontally (vertically) polarized by XG.) Because we have two optical paths after XG, we need two of P2 (P2h and P2v). The converging beams from P2h and P2v are sent to the beam combiner, BC, through a 90° reflection by grids Gh and Gv. The reason for using grids instead of mirrors here will be explained in the next subsection. BC is composed of two flat mirrors, which will deflect the corresponding beams by 89.8° in the horizontal direction. After two more reflections by flat mirrors (F4 and F5), the two beams will be sent toward SHARC II. The Nasmyth focus is re-imaged at BC, where the optical distance to the detector array is the same as that from the original Nasmyth focus in the original SHARC-II optical path.

Note that after the "combiner", the two beams are still shifted apart a little horizontally so they will head to different halves of the detector array. For the original chief ray of SHARC II, the separation of the split dual beams will be 20 pixels on the detector array. We do not use the central 8 × 12 pixels which might be reached by both channels (in case of misalignment, diffraction, etc). Thus each subarray includes 12 × 12 pixels. Given that SHARC II has pixel size of 4.6"×4.6", the field of view of SHARP is ~ 55" × 55". The 89.8° reflection at BC is calculated so that the two shifted channels still pass through the cold stop at the pupil inside the SHARC II cryostat.

The polarimeter can be easily removed from the optical path by removing P1 and F5. Thus, the modular design (Fig. 6) makes it easy to switch between camera and polarimeter, by removing only "Box 4".

2.4 The cold load

The light from the sky that enters XG after passing through HWP is not the only radiation entering XG. Noise (e.g. thermal emission from Box 3) enters XG from the opposite side (Fig. 6). This noise must be prevented from getting into SHARC II. XG also divides the noise into two polarized components, and note that they will be orthogonal to the signals from the sky. The reason we use grids in Gh and Gv (Fig. 5) is to reflect only the signals and filter out the noise that gets into the system from the "wrong" side of XG. Gh and Gv alone will not solve the problem, because the detectors can still "look" through these grids and see the emission from anything located behind the grids. Gh and Gv are coupled with a pair of paraboloidal mirrors (P_3h and P_3v, Fig. 5), whose focal length was chosen such that, through them, the detectors will look back into the cryostat, where the thermal emission is much lower.

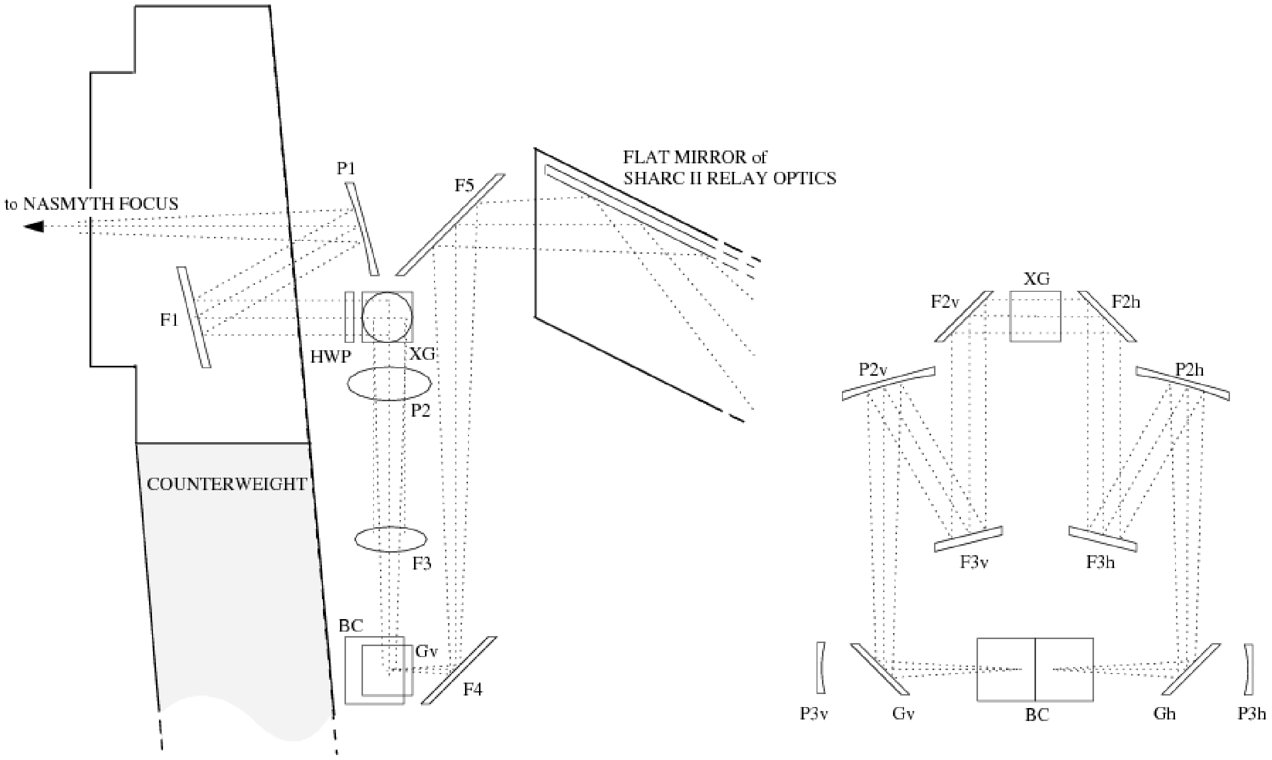

Fig. 5. Two views of SHARP. Left: The expanding beam from the Nasmyth focus is reflected by paraboloid P1 and by a flat mirror at F1, passes through the half-wave plate HWP, and reaches the crossed grid XG. From XG, the horizontal polarization component propagates into the plane of the paper while the vertical component is directed towards the viewer. Right: View towards the Nasmyth focus. Vertical and horizontal components leaving the crossed grid undergo further reflections by mirrors and grids (F2v-F3v-P2v-Gv and F2h-F3h-P2h-Gh, respectively), ultimately bringing the components back together at the beam combiner BC which directs the recombined image towards the viewer. (BC consists of two mirrors joined at 89.8° to form a roof–shaped optical surface.) After reflection by BC, the two orthogonal polarizations are displaced laterally. The left view shows this reconstituted image being directed into the relay optics by flats F4 and F5. P1 and P2h (or P2v) form a pair of crossed paraboloids[16]. SHARC-II is easily converted back to photometric mode by removing P1 and F5.

Fig. 6 The modular design of SHARP. The components in each box are: Box 1− P3h/v, Gh/v, F4, and BC; Box 2− P2h/v and F3h/v; Box 3− F1, HWP, XG, and F2h/v; Box 4 − P1 and F5.

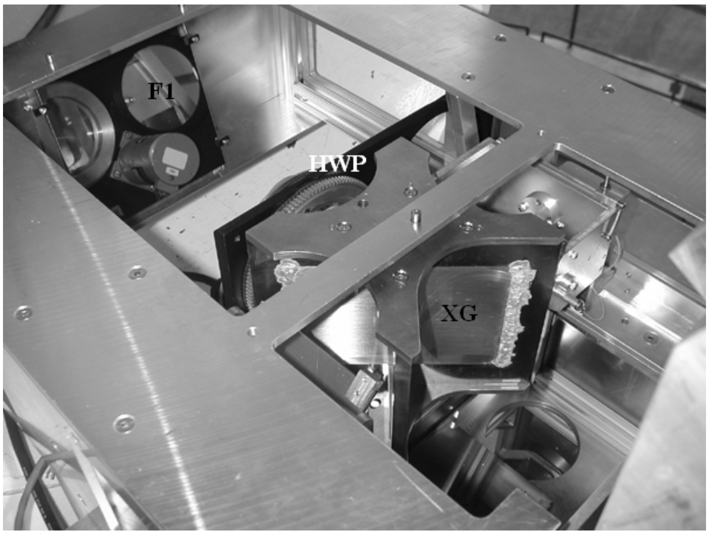

Fig. 7 F1, HWP, and XG in Box 3. F1 is the large square mirror, where the reflection of the half-wave plate module (HWP) can be seen. This reflection shows the mounting positions for the two half-wave plates (only one has a plate installed) and also the stepping motor. The signals pass through the HWP toward XG where they are divided into two orthogonal polarization components that are sent in opposite directions. Noise will also enter XG, from the opposite direction. The noise will be filtered out by Gh/v in Box 1(see discussion in section 2.4).

3. PERFORMANCE

Here we summarize the predicted performance of SHARP and the actual measurements acquired during CSO runs in August 2005 and January 2006.

3.1 Beam size

The beam FWHM of SHARC-II is 9” at 350 μm. Based on ZEMAX simulations, the polarimeter module should not degrade this performance significantly[23]. Mars is the main target we used for testing the beam size. Note that Mars is not a point source, so we have to compare with the size of Mars as seen by SHARC-II.

In August 2005, the FWHM of Mars was 10” in the h channel (Fig. 5), the same as we should expect from SHARC II. But the v channel obtained an elongated beam with the long axis twice as large as the short axis. This was due to the construction of XG: the horizontal grid is constructed as one piece while the vertical grid is composed of two, one on each side of the horizontal grid. The elongation was due to a misalignment between the two pieces of the vertical grid. We verified this idea by replacing XG with a single vertical grid, which produced the same good image quality in the v channel as we saw in the h channel when using XG.

In fall 2005, XG was repaired by QMCI. The two beams showed the same FWHM in January 2006. However, during data analysis after the run, we found that both beams are elongated ~30% in a direction that varies with elevation. We suspect that the elongation is caused by misalignment of M3, M4, or M5, because we were not as successful in carrying out the alignment of these mirrors in January 2006 as we had been in August 2005. We conclude that the beam size difference between SHARP and SHARC II is negligible, but the whole system needs to be well aligned.

3.2 Throughput

For each channel of SHARP, 10 reflections are added to the original CSO/SHARC II system. To reduce absorption of the reflecting components, we gold-coat all mirrors except for P1, P2, and BC, which are made of solid aluminum. The average absorption for these surfaces should be below 0.5%. The surface error in P1 and P2 is about 5 μm rms, which will give another 3% inefficiency (Ruze losses) for each curved mirror (Flat mirrors are all of optical quality.) We also expect a 5% efficiency loss due to grid imperfections.

The biggest inefficiency comes from the HWP, which has 5-10 % absorption due to the half-wave plate[25] and another 2% loss due to imperfections in the a/r coatings.

By sizing all the SHARP optical elements so as to preserve five Airy rings, we have reduced the diffraction losses to very low levels. The ZEMAX simulations indicate that these are below 1%.

Summing all the losses up, we predicted the net transmission of SHARP relative to SHARC-II as ~ 77%. In January 2006, the efficiency was measured at 75%. This measurement was achieved by observing Mars with and without SHARP installed and comparing the flux integrated over all pixels. (For the purposes of making this comparison, it is also necessary to make a responsivity correction.)

3.3 Instrument polarization

We estimate the instrument polarization (i.p.) by assuming all the planets we observed (Mars, Saturn, and Jupiter) in January 2006 are unpolarized. The estimate can be improved later by taking the small polarization of planets into account when more data are collected.

The results are summarized in Figures 8 and 9. As explained in the caption to Figure 8, we model the instrumental polarization (i.p.) as the sum of two components. One is fixed with respect to SHARP, and one is presumed to vary with telescope elevation, as would be expected for polarization induced by the reflection at M3. In the submillimeter, reflection from aluminum mirrors will be several tenths of a percent polarized perpendicular to the plane defined by the incident and reflected beams[26]. The fixed i.p. contains contributions due to the reflections at P1 and F1, where the main beam is propagated within a vertical plane so the induced polarization should be horizontal. The i.p. due to M3 should be horizontal when the telescope is looking at the zenith (Fig. 1), and should rotate clockwise as the telescope drops to the horizon. In Figure 8 it can be seen that, for both i.p. components, the angle we measure is approximately consistent with these expectations.

4. FUTURE PLANS

In addition to improving the measurements of beam size and i.p. discussed in previous section, several analysis tasks are ongoing and should be finished before our next observing run in July 2006.

1．Signal-to noise evaluation:
SHARC-II achieves a 1σ r.m.s. error of 24 mJy in one hour of observations[20, 28]. Using this figure while taking into account the throughput, the inefficiency of using the chop/nod mode[20], the time to measure both Q and U, and the slightly better duty cycle for polarimetry as compared with photometry that requires frequent total power calibration (60% and 50%, respectively), we calculate that a point source with a 350 μm flux of 2.7 Jy is required in order to obtain in five hours a polarization measurement having a polarization error of 1%. This assumes low zenith angle and good submillimeter weather, as discussed on the SHARC-II web page[28]. Preliminary analysis suggests that we have roughly achieved this sensitivity, but a more careful study is underway.

2. Analysis of January 2006 science data:
During our second run in January 2006, we had several days of good submillimeter weather (230 GHz atmospheric opacity about 0.05). Besides the work on planets described above, we observed Orion-KL, B1, and M82. For Orion-KL, in about 20 minutes were able to detect polarization at several dozen positions. The results are consistent with previous Hertz observations that were made at the same wavelength but with lower spatial resolution[27]. Analysis of data for B1 and M82 is still under way. In Figure 10 we show separate maps of M82 made with the h channel and the v channel, and we compare these to a photometric map made with the Hertz polarimeter, illustrating the improvement in spatial resolution. Preliminary results for M82 show that for bright parts of the galaxy we achieve low errors (< 1%) but also low polarization ($\lesssim$ 2%).

3. Data analysis method for extended sources:
The sources we observed so far are all relatively compact so they can be covered by SHARP's 55" × 55" field of view. This gives us a way to measure the sky noise residual with the off-source pixels to improve the sensitivity. We are developing a new data analysis method for extended sources.

This project is funded by NSF awards to Northwestern University and to The University of Chicago; and by NSERC awards to The University of Western Ontario.

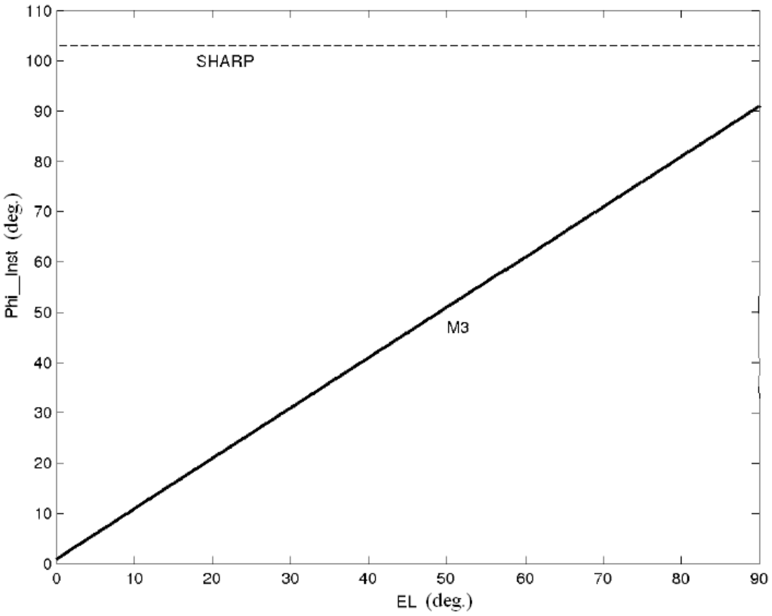

Fig. 8 Angle of polarization determined for the two components of instrument polarization (i.p.). One component is presumed to be fixed with respect to SHARP while another is fixed with respect to M3. Thus, four free parameters (P and Phi for the two components of i.p.) were determined from a least-squares fit to polarization measurements of planets, presumed unpolarized. The dashed line corresponds to the component that is fixed with respect to SHARP, which has a magnitude of P = 0.46 % and a fixed angle of polarization of Phi_Inst = 103 degrees. (Phi_Inst is measured from the vertical, increasing counter-clockwise as viewed by an observer standing at the postion of Box 4 and looking down the Nasmyth tube toward M3.) The solid line shows the value of Phi_Inst for the component of i.p. that is fixed with respect to M3. This component has a magnitude of 0.42 % and an angle Phi_Inst that varies with elevation as shown. For this component of i.p., the fit gives an angle of polarization that lies within one degree of that predicted by the classical skin effect theory applied to M3. The angle for the fixed component of i.p. is consistent (within 13 degrees) with polarization due to classical skin effect at P1 and F1.

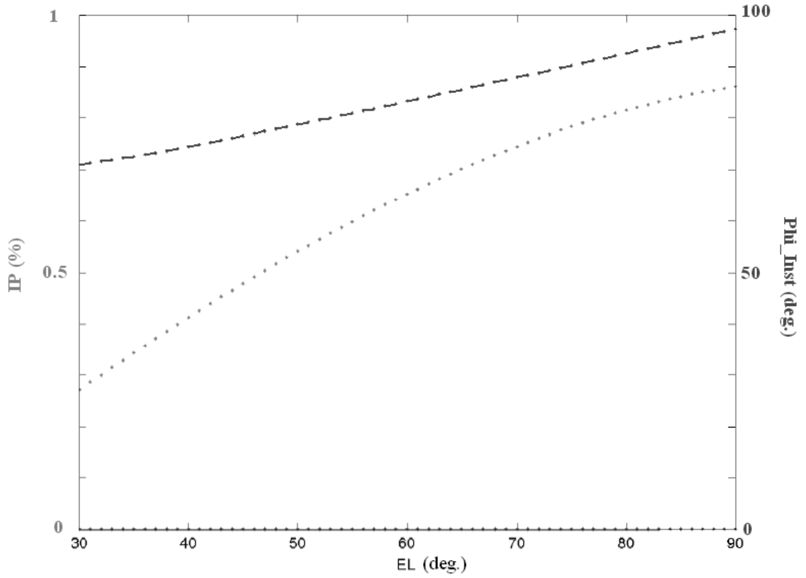

Fig. 9 The degree (dotted line) and angle (dashed line) of instrumental polarization (i.p.). This i.p. results from two components, as discussed in the caption to Figure 8; here we show the total i.p. The angle (Phi_Inst) is measured in instrument coordinates. The abscissa is telescope elevation. Phi_Inst is measured with respect to the vertical, as discussed in the caption to Figure 8.

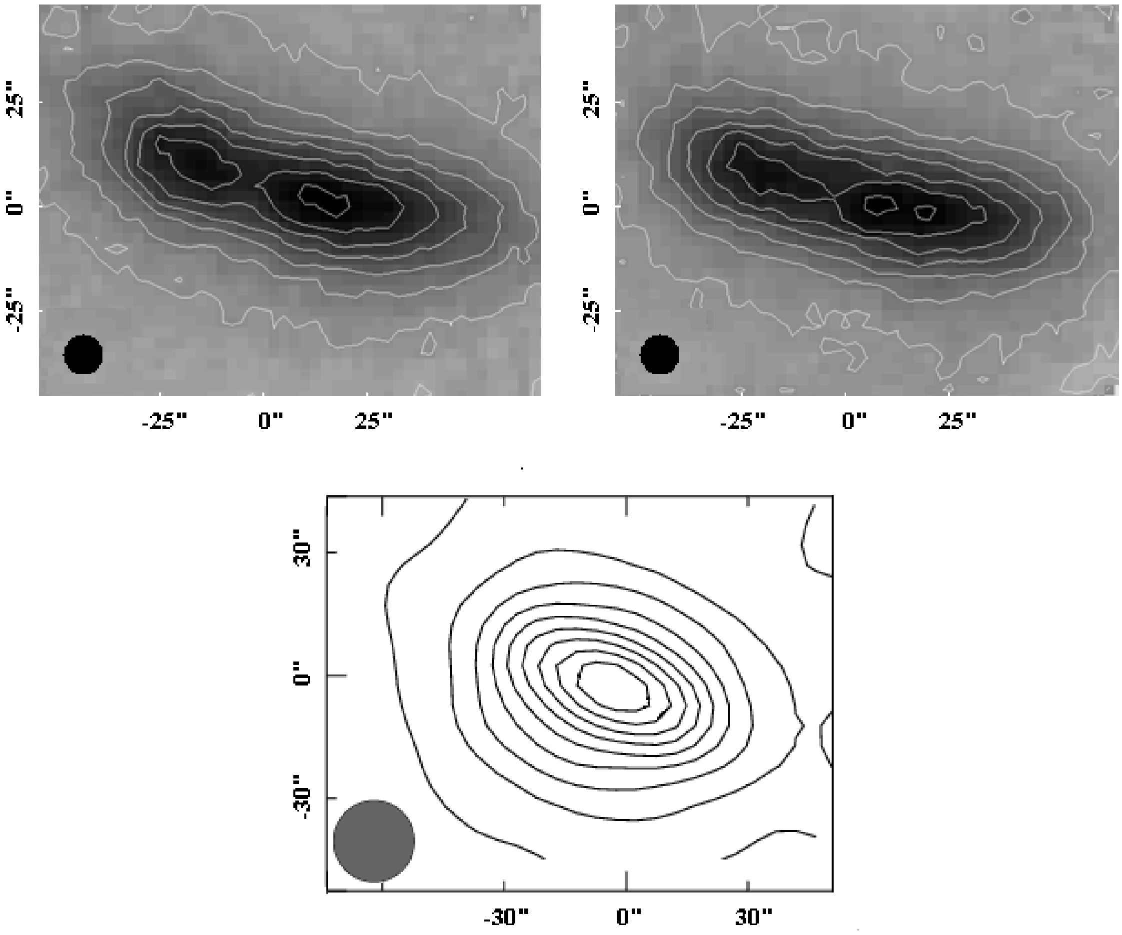

Fig. 10 Top: images of M82 observed by the two polarization channels of SHARP. Polarimetry data analysis is underway. Bottom: photometric map of M82 measured by our previous CSO polarimeter, Hertz. The circles in the lower left corners show the beam sizes. The SHARP images reveal much more detail.

REFERENCES

1. Cudlip, W., Furniss, I., King, K.J., Jennings, R.E. 1982, “Far infrared polarimetry of W51A and M42”, MNRAS, 200, 1169
2. Hildebrand, R.H., Dragovan, M., & Novak, G. 1984, “Detection of submillimeter polarization in the Orion Nebula”, ApJ, 284, L51
3. Platt, S.R., Hildebrand, R.H., Pernic, R.J., Davidson, J.A., & Novak, G., 1991, “100-micron array polarimetry from the Kuiper Airborne Observatory - Instrumentation, techniques, and first results”, PASP, 103, 1193
4. Schleuning, D.A., Dowell, C.D., Hildebrand, R.H., Platt, S.R., & Novak, G. 1997, “HERTZ, A Submillimeter Polarimeter”, PASP, 109, 307
5. Dowell, C.D., Hildebrand, R.H., Schleuning, D.A., Vaillancourt, J.E., Dotson, J.L.,Novak, G., Renbarger, T., & Houde, M. 1998, “Submillimeter Array Polarimetry with Hertz”, ApJ, 504, 588

6. Hildebrand, R.H., Dotson, J.L., Dowell, C.D., Novak, G., Schleuning, D.A., Vaillancourt, J.E. 1998, “Hertz: an imaging polarimeter”, in “Advanced Technology MMW, Radio, and Terahertz Telescopes”, Ed. T.G. Phillips, SPIE Proc. Ser., 3357, 289
7. Hildebrand, R.H., Davidson, J.A., Dotson, J.L., Dowell, C.D., Novak, G., &Vaillancourt, J.E. 2000, “A Primer on Far-Infrared Polarimetry”, PASP, 112, 1215. (Erratum: 112, 1621)
8. Dotson, J.L., Davidson, J.A., Dowell, C.D., Schleuning, D.A., & Hildebrand, R.H. 2000, “Far-Infrared Polarimetry of Galactic Clouds from the Kuiper Airborne Observatory”, ApJS, 128, 335
9. Greaves, J. S. et al., “A Submillimeter Imaging Polarimeter at the James Clerk Maxwell Telescope”, MNRAS 340, 353, 2003.
10. Holland, W. S.et al. “SCUBA: a common-user submillimetre camera operating on the James Clerk Maxwell Telescope”, 1999, MNRAS, 303, 659.
11. Tamura, M. et al. “First Detection of Submillimeter Polarization from T Tauri Stars”, 1999,ApJ, 525, 832
12. Moran, J. M., “Submillimeter array”, 1998, SPIE, 3357, 208.
13. Marrone, D. P, Moran, J. M, Zhao, J.-H, Rao, R., “Interferometric Measurements of Variable 340 GHz Linear Polarization in Sagittarius A*”, astro-ph/0511653
14. Renbarger, T. et al., “Early Results from SPARO: Instrument Characterization and Polarimetry of NGC 6334”, PASP 116, 415-424, 2004.
15. Novak, G. et al., “First Results from the Submillimeter Polarimeter for Antarctic Remote Observations: Evidence of Large-scale Toroidal Magnetic Fields in the Galactic Center”, Ap J, 583, 83, 2003.
16. Li, H., Calisse, P. G, Chuss, D. T, Griffin, G. S, Krejny, M., Loewenstein, R. F, Newcomb, M. G., and Novak, G., “Results of SPARO 2003: Mapping Magnetic Fields in Giant Molecular Clouds”, ApJ, in press.
17. Kovac, J. M.; Leitch, E. M.; Pryke, C.; Carlstrom, J. E.; Halverson, N. W.; Holzapfel, W. L., “Detection of polarization in the cosmic microwave background using DASI”, 2002, Natur., 420, 772
18. Benoit, A. et al. “First detection of polarization of the submillimetre diffuse galactic dust emission by Archeops”, 2004, A&A, 424, 571.
19. Page, L. et al., “Three Year Wilkinson Microwave Anisotropy Probe (WMAP) Observations: Polarization Analysis”, astro-ph/0603450
20. Dowell, C. D, et al. “SHARC II: a Caltech submillimeter observatory facility camera with 384 pixels", 2005, in Proc. SPIE 4855: Millimeter and Submillimeter Detectors for Astronomy, eds. T. G. Phillips & J. Zmuidzinas, 73.
21. Li, H., Calisse, P. G, Chuss, D. T, Griffin, G. S, Krejny, M., Loewenstein, R. F.,, Newcomb, M. G., and Novak, G., “Results of SPARO 2003: Data Analysis and Polarization Maps”, 2005, in Astronomical Polarimetry - Current Status and Future Directions, ASP Conf. Ser. 343, Eds. A. Adamson, C. Aspin, C. J. Davis, and T. Fujiyoshi (San Francisco: ASP) p. 43.
22. Kirby, L.; Davidson, J. A.; Dotson, J. L.; Dowell, C.D.; Hildebrand, R. H. “Improved Data Reduction for Far-Infrared/Submillimeter Polarimetry”, 2005, PASP, 117, 991.
23. Novak, G. et al. “A polarimetry module for CSO/SHARC-II”, 2004, SPIE 5498, 278.
24. Serabyn, E. 1995, “Wide-Field Imaging Optics for Submm Arrays," in ASP Conf. Ser. 75: Multi-Feed Systems for Radio Telescopes, eds. D. T. Emerson & J. M. Payne, 74.
25. Murray, A. G., Flett, A. M., Murray, G., & Ade, P. A. R. 1992, “High efficiency half-wave plates for submillimetre polarimetry” Infrared Physics, 33, 113.
26. Renbarger, T., Dotson, L., J., Novak, G., “Measurement of submillimeter polarization induced by oblique reflection from aluminum alloy”, 1998, Applied Optics, 37, 28.
27. Schleuning, D. A., “Far-Infrared and Submillimeter Polarization of OMC-1: Evidence for Magnetically Regulated Star Formation”, 1998, ApJ, 184, 349.
28. SHARC-II website: http://www.submm.caltech.edu/~sharc/general/overview.html